Structural Engineering and Mechanics, Vol. 5, No. 5 (1997) 663-677
DOI: http://dx.doi.org/10.12989/sem.1997.5.5.663

Improved numerical approach for the bond-slip behavior under cyclic loads

H.G. Kwak†

Department of Civil Engineering, Korea Advanced Institute of Science and Technology, Taejon 305-701, Korea

Abstract. Bond-slip behavior between reinforcement and concrete under push-pull cyclic loadings is numerically investigated based on a reinforcement model proposed in this paper. The equivalent reinforcing steel model considering the bond-slip effect without taking double nodes is derived through the equilibrium at each node of steel and the compatibility condition between steel and concrete. Besides a specific transformation algorithm is composed to transfer the forces and displacements from the nodes of the steel element to the nodes of the concrete element. This model first results in an effective use in the case of complex steel arrangements where the steel elements cross the sides of the concrete elements and second turns the impossibility into a possibility in consideration of the bond-slip effect in three dimensional finite element analysis. Finally, the correlation studies between numerical and experimental results under the continuously repeated large deformation stages demonstrate the validity of developed reinforcing steel model and adopted algorithms.

Key words: cyclic loading; bond-slip; double node; nonlinear analysis; embedded steel.

1. Introduction

It is well known that the load carrying capacity of reinforced concrete (RC) structure depends on the bond between reinforcing steel and concrete; nevertheless, all design procedure is based on insuring that bond failure does not occur even upon overload, that is, complete compatibility between concrete and reinforcement which means perfect bond is usually assumed (Choi and Kwak 1990). But this assumption is only valid in those regions where no or only negligible stress transfer between the two materials occurs. In regions of high stresses in the contact interfaces such as near cracks, however, the bond stresses are related to relative displacements between concrete and reinforcing steel. The assumption of perfect bond in cracked zones would cause infinitely high strains to explain the existence of a finite crack width. In reality, there are different strains in the adjacent regions of the connections between reinforcing steel and concrete (Fig. 1). Moreover since the shear stresses transferred across interfaces in concrete such as crack surfaces and bond surfaces have a significant influence on the behavior of concrete structures, the response of RC structures in which shear plays an important role, such as over-reinforced beams and shear wall, is much more affected by the bond-slip of reinforcing steel (Kwak and Filippou 1995).

To account for the bond-slip of reinforcing steel two alternative approaches have been proposed

† Assistant Professor

in the finite element analysis of reinforced concrete structures. The first approach makes use of the bond-link element proposed by Ngo and Scordelis (1967). This element connects a node of a concrete finite element with a node of an adjacent steel element. The link element has no physical dimensions, i.e., the two connected nodes have the same coordinates. A bond-link can be thought to consist of three springs, one parallel and the other two normal to the longitudinal axis of the reinforcing steel. The second approach makes use of the bond-zone element developed by de Groot, *et al.* (1981). In this element the behavior of the contact surface between steel and concrete and the behavior of the concrete in the immediate vicinity of the reinforcing bar is described by a material law which considers the special properties of the bond zone. The contact element provides a continuous connection between reinforcing steel and concrete, if a linear or higher order displacement field is used in the discretization scheme. Even though many studies of the bond-slip relationship between reinforcing steel and concrete have been conducted, considerable uncertainty about this complex phenomenon still exists because of the many parameters which are involved. Especially the complication in numerical modeling caused by taking the double nodes exacts that most finite element studies of RC structures do not account for bond-slip of reinforcing steel.

In this study, an equivalent reinforcing steel model which can consider the bond-slip without taking the double nodes is proposed and a specific transformation algorithm to solve the constructed global equilibrium equation for each steel element is introduced. Moreover correlation studies between analytical and experimental results are conducted with the objective to establish the validity of the proposed model under monotonically increasing loads and repeated cyclic loads.

2. Numerical modeling of bond-slip behavior

2.1. Bond-slip

Since bond behavior is the interaction between reinforcing steel and surrounding concrete and can be thought of as the shear stress or force between the two materials, it is influenced by the stress levels in the bars and conditions of concrete around the bars. Moreover, bond stresses in reinforced concrete members arise from the change in the steel force along the length and the effect of bond becomes more pronounced at the end anchorages of reinforcing bars

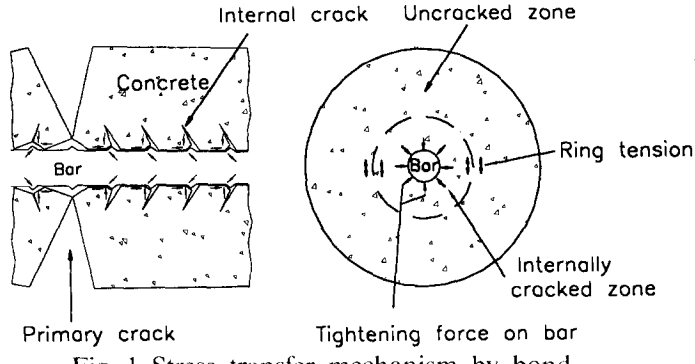

Fig. 1 Stress transfer mechanism by bond.

and in the vicinity of cracks because the force in the reinforcing steel is transmitted to the concrete by bond, or vice versa (Fig. 1).

Two basically different elements, namely, the bond-link element and bond-zone element, have been proposed to date for inclusion of the bond-slip effect in the finite element analysis of RC structures as mensioned above. In studies where the detailed local behavior is of interest, the continuous bond elements such as bond-zone elements are most appropriate. In cases, however, where the overall structural behavior is of primary interest, the bond-link element provides a reasonable compromise between accuracy and computational efficiency. Therefore, the bond-link element is selected for representing the bond-slip effect in this study.

However, the use of bond-link element imposes the following restrictions on the finite element mesh: (1) each reinforcing bar must be located along the edge of a concrete element, and (2) a double node is required to represent the relative slip between reinforcing steel and concrete. The bond stress at a certain location can thus be determined from the relative displacement between concrete and steel. These previous restrictions lead to a considerable increase in the number of nodes and elements in the case of complex structure, not only because of doubling the number of nodes along the reinforcing steel bars, but also because the mesh has to be tailored around the reinforcement layout. The complexity of mesh definition and the large number of degrees of freedom has discouraged researchers from including the bond-slip effect in many previous studies. To address some of these limitations of the bond-link element, an equivalent reinforcing steel model considering the bond-slip effect without taking the double nodes is proposed by condensing the steel nodes internally.

2.2. Adopted material properties

The properties of reinforcing steel, unlike concrete, are generally not dependent on environmental conditions or time and for all practical purposes steel can be assumed to exhibit the same stress-strain curve in compression as in tension. Thus the specification of an uniaxial stress-strain relation for steel is sufficient to define the material properties needed without introducing the complexities of three-dimensional constitutive relations in the analysis of reinforced concrete structures since the reinforcing steel is used in the concrete construction in the form of reinforcing bars or wire. In this study the reinforcing steel is modeled with discrete one-dimensional truss elements embedded in the concrete element. This representation of steel can be easily superimposed on the two-dimensional concrete element mesh where the nodes of the steel element do not coincide with the nodes of the concrete element. A significant advantage of the discrete representation, in addition to its simplicity, is that it can include the slip of reinforcing steel with respect to the surrounding concrete. Besides to simulate the material property according to the loading history, the stress-strain relation proposed by Menegotto and Pinto (1973), which can simulate effectively the material behavior under the initial yielding and also large deformation stage after yielding, is adopted (Fig. 2). The basic stress-strain relation in the adopted model can be expressed as fellows:

$$\sigma^o = b \cdot \varepsilon^o + \frac{(1-b) \cdot \varepsilon^o}{(1+\varepsilon^{oR})^{1/R}} \tag{1}$$

where $\varepsilon^o = (\varepsilon - \varepsilon_r)/(\varepsilon_o - \varepsilon_r)$, $\sigma^o = (\sigma - \sigma_r)/(\sigma_o - \sigma_r)$, $b = E_o/E_t$ is the strain hardening parameter, $R = R_o - a_1\zeta/(a_2 + \zeta)$ is the material constant to simulate the Bauschinger effect and the stress

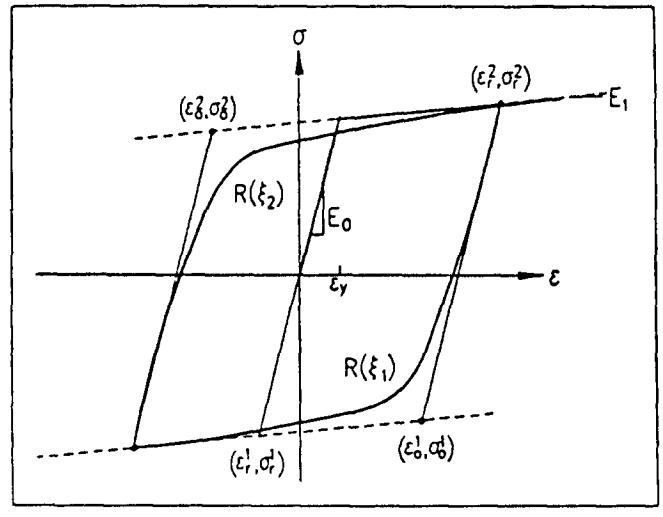

Fig. 2 Stress-strain relation of steel.

history, ζ expressed as the ratio between the yield strain and $\varepsilon_o - \varepsilon_r$ is the parameter representing the strain history, and the values of material constants $R_o = 20$, $a_1 = 18.5$, $a_2 = 0.15$ obtained from the experimental study are used in this study.

To account for the bond-slip effect it is necessary to construct a constitutive relationship between bond stress and bond slip at representative location along the reinforcing steel. The bond stress is determined from the change in steel stress over a certain measurement length, which is usually taken equal to five bar diameters, and the relative slip is determined externally or internally. It is, therefore, practically impossible to establish a local bond stress-slip relation since the measured bond stress-slip relation generally represents the average relation over the measurement length. Moreover, the result is very sensitive to the experimental error because the bond stress is derived from the change in steel stress, and the bond-slip relation also depends on the position of the bars, the surface conditions of bars, the loading stage, the boundary conditions, and the anchorage length of bars. In spite of these difficulties, several experimental bond-stress slip relations have been proposed (Eligehausen, *et al.* 1983, ASCE 1982). There are also many simple relations among the proposed models due to these difficulties (ASCE 1982). Since it is the objective of this study to investigate the bond-slip behavior of reinforcing steel in more detail, a more sopisticated bond-slip model is adopted in the correlation studies of anchored reinforcing bars under monotonic and cyclic loads as shown in Fig. 3. These explicit expressions for bond stress-slip relation are presented by Eligehausen, *et al.* (1983) based on many experiments and modified to improve an initial bond-slip behavior by Zulfiqar and Filippou (1990). The monotonic envelope consists of an initial nonlinear relation $\tau = \tau_1 (u/u_1)^\alpha$, valid for $u \le u_1$, followed by a plateau $\tau = \tau_1$ for $u_1 \le u \le u_2$. For $u \ge u_2$, τ decreases linearly to the value of ultimate frictional bond resistance τ_3 at a slip value of u_3 which is assumed to be equal to the clear distance between the lugs of deformed bars. As the unloading (curve c in Fig. 3) and reloading (curve d in Fig. 3) are repeated, the monotonic envelopes are updated (curve e in Fig. 3) by reducing the characteristic bond stress values τ_1 and τ_3 by a factor which is a function of the damage parameter d. The damage parameter has the following form.

$$\tau_1(N) = \tau_1(1-d) \tag{2}$$

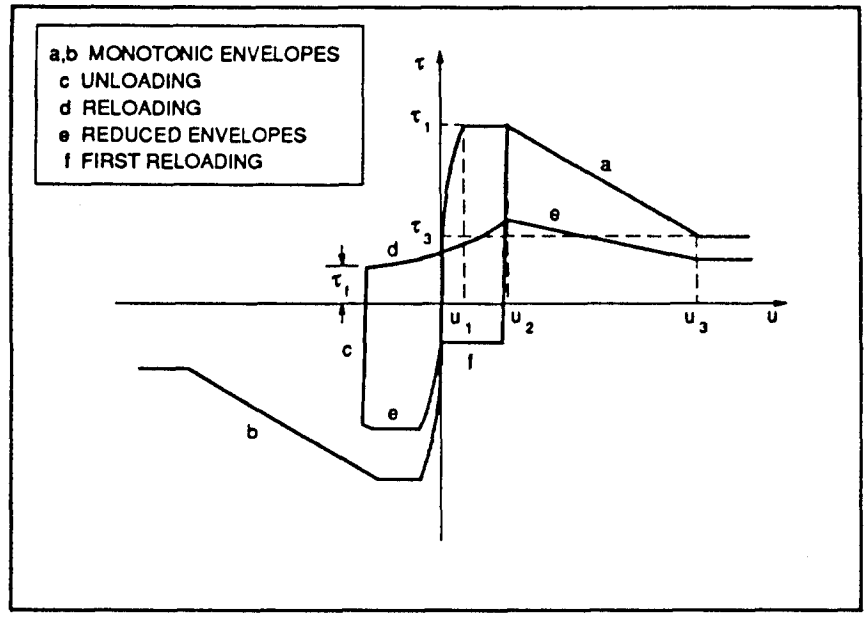

Fig. 3 Bond stress-slip relation.

where τ_1 is the characteristic value of the virgin envelope curve and $\tau_1(N)$ is the corresponding value after N cycles. The damage parameter depends on the total energy dissipated by the bond-slip process and is given by $d=1-e^{-1.2(E_i/E_o)^{1.1}}$ where E is the total dissipated energy, E_o is the energy absorbed under monotonically increasing slip up to the value u_3 and is used as a normalization parameter. More details can be found elsewhere (Viwathanatepa, *et al.* 1979).

2.3. Embedded reinforcing steel bond element

Based on the aforementioned material models, an equivalent reinforcing steel element which can consider the bond-slip effect in spite of embedding in concrete element is proposed. Unlike the classical bond models, the proposed model is considering the bond-slip effect without taking double nodes by condensing out the steel nodes at the structural level. This requires separate treatment of the entire reinforcing bar. To explain the derivation procedure a convenient free body diagram is selected which isolates the steel element with the bond-link elements attached at its end points as shown in Fig. 4. Fig. 4b shows the element before and Fig. 4c after deformation. In Fig. 4, i and j denote the end points of the element, points 1 and 3 are associated with concrete and points 2 and 4 are associated with the reinforcing steel at ends i and j, respectively. The corresponding degrees of freedom of the reinforcing steel and concrete at each end are connected by the bond-link element whose stiffness depends on the relative displacewment between steel and concrete. With this assumption the stiffness matrix which relates the end displacements along the axis of the reinforcing bar with the corresponding forces can be expressed as follows:

$$\begin{Bmatrix} P_c \\ P_s \end{Bmatrix} = \begin{bmatrix} K_{cc} & K_{cs} \\ K_{cs} & K_{ss} \end{bmatrix} \cdot \begin{Bmatrix} d_c \\ d_s \end{Bmatrix} \tag{3}$$

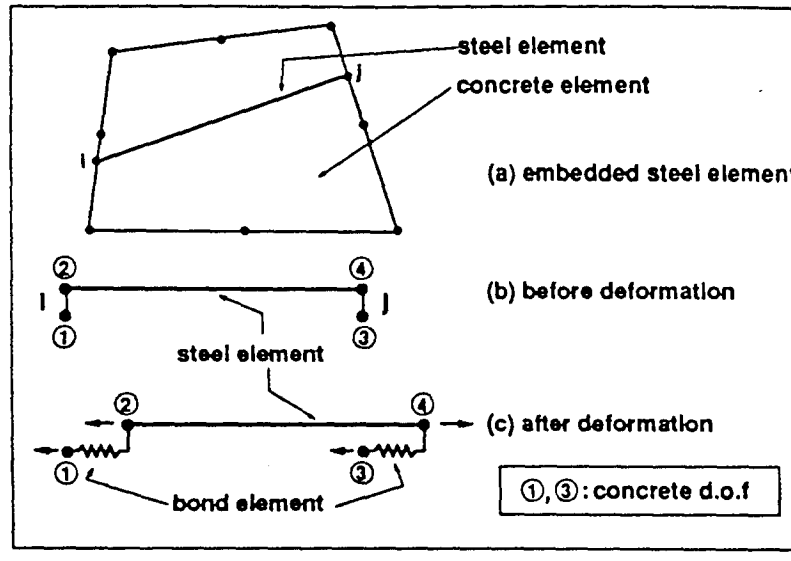

Fig. 4 Discrete reinforcing steel element with bond-slip.

where

$$\boldsymbol{K}_{cc}=\begin{bmatrix} K_{bi} & 0 \\ 0 & K_{bj} \end{bmatrix},\quad \boldsymbol{K}_{cs}=\begin{bmatrix} -K_{bj} & 0 \\ 0 & -K_{bj} \end{bmatrix},\quad \boldsymbol{K}_{ss}=\begin{bmatrix} K_{ss}+K_{bi} & -K_{s} \\ -K_{s} & K_{ss}+K_{bj} \end{bmatrix} \tag{4}$$

$k_s=AE/L$ is the steel stiffness, $k_b=E_bA=E_bm\pi d_bL/2b$ is the stiffness of the bond-link parallel to the bar axis at the corresponding end of the steel element where the dowel action is neglected, E_b is the slip modulus, A is the bar circumferential area tributary to one bond link element, m is the number of bars of diameter, d_b is the diameter of reinforcing bar, L is the spacing of the bond links along the reinforcing bar, and b is the width of the member cross section. The factor 2 appears in the denominator to account for the fact that it is usually convenient to place bond-link element at both the top and bottom of the reinforcing bar element (ASCE 1982).

Since the finite element model only includes the concrete displacement degrees of freedom, the degrees of freedom which are associated with the reinforcing steel need to be condensed out from the element stiffness matrix before it is assembled into the structure stiffness matrix. By applying static condensation of the steel degrees of freedom in Eq. (3) the following relation between concrete displacements and corresponding forces results in:

$$\{\boldsymbol{P}_c^*\}=[\boldsymbol{K}_{cc}^*]\cdot\{\boldsymbol{d}_c\} \tag{5}$$

where

$$\{\boldsymbol{P}_c^*\}=\{\boldsymbol{P}_c\}-[\boldsymbol{K}_{cs}]\cdot[\boldsymbol{K}_{ss}]^{-1}\cdot\{\boldsymbol{P}_s\} \tag{6}$$

$$[\boldsymbol{K}_{cc}^*]=[\boldsymbol{K}_{cc}]-[\boldsymbol{K}_{cs}]\cdot[\boldsymbol{K}_{ss}]^{-1}\cdot[\boldsymbol{P}_{cs}] \tag{7}$$

After some calculations for evaluating the inverse and carrying out the multiplications the equivalent concrete element stiffness matrix $[\boldsymbol{K}_{cc}^*]$ can be expressed as:

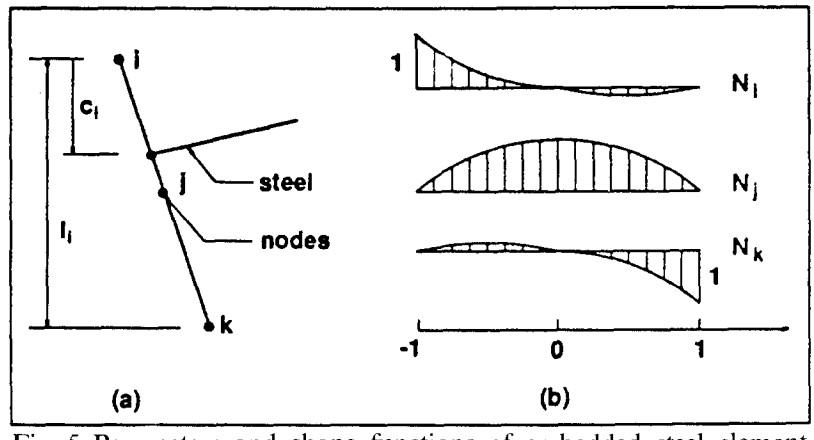

Fig. 5 Parameters and shape functions of embedded steel element.

$$[K_{cc}^{*}]=\frac{k_s\cdot k_{bi}\cdot k_{bj}}{k_s\cdot(k_{bi}+k_{bj})+k_{bi}\cdot k_{bj}}\cdot\begin{bmatrix}1 & -1\\ -1 & 1\end{bmatrix}=[K_{eq}]_s \tag{8}$$

which is the local stiffness matrix of the reinforcing steel element including the effect of bond-slip and it is now apparent that bond slip reduces the stiffness of the reinforcing steel element. In case of perfect bond the bond stiffness terms k_{bi} and k_{bj} become infinitely large and the stiffness matrix in Eq. (8) is reduced to the local stiffness of the embedded steel model with perfect bond.

Since the end points of the reinforcing bar element do not generally coincide with the nodes of the concrete element, the steel element stiffness matrix of Eq. (8) expressed relative to the global coordinate system by applying a rotation matrix has to undergo another transformation before it can be assembled together with the concrete element stiffness matrix. This can be formally expressed by the following relation:

$$[K_{GL}]=[T_2]^T\cdot[T_1]^T\cdot[K_{eq}]_s\cdot[T_1]\cdot[T_2] \tag{9}$$

where $[K_{eq}]_s$ denotes the local stiffness matrix of the axially loaded reinforcing bar derived in Eq. (8) and $[T_1]$ represents the transformation matrix to the global coordinate system expressed by the following relation:

$$[T_1]=\begin{bmatrix}\cos\theta & \sin\theta & 0 & 0\\ 0 & 0 & \cos\theta & \sin\theta\end{bmatrix} \tag{10}$$

Transformation matrix $[T_2]$ can be derived with the procedure used to establish the consistent nodal forces of the finite element method. When the 8-node isoparametric element is used in the two-dimensional mesh representation of the member, the shape functions for nodes i, j, k in Fig. 5 are $N_i=(r_i-1)\cdot(2r_i-1)$, $N_j=4r_i\cdot(1-r_i)$, $N_k=r_i\cdot(2r_i-1)$ where $r_i=c_i/l_i$(Fig. 6). If the reinforcing bar element crosses the concrete element boundary on sides 2 and 4 in Fig. 6, nodes i, j and k correspond to node numbers 1, 8, and 7 on side 4 and node numbers 3, 4 and 5 on side 2, respectively. With the notation of Fig. 6 the transformation matrix $[T_2]$ has the following form:

$$[T_2]=\begin{bmatrix}A_1 & 0 & 0 & 0 & 0 & 0 & A_3 & A_2\\ 0 & 0 & B_1 & B_2 & B_3 & 0 & 0 & 0\end{bmatrix} \tag{11}$$

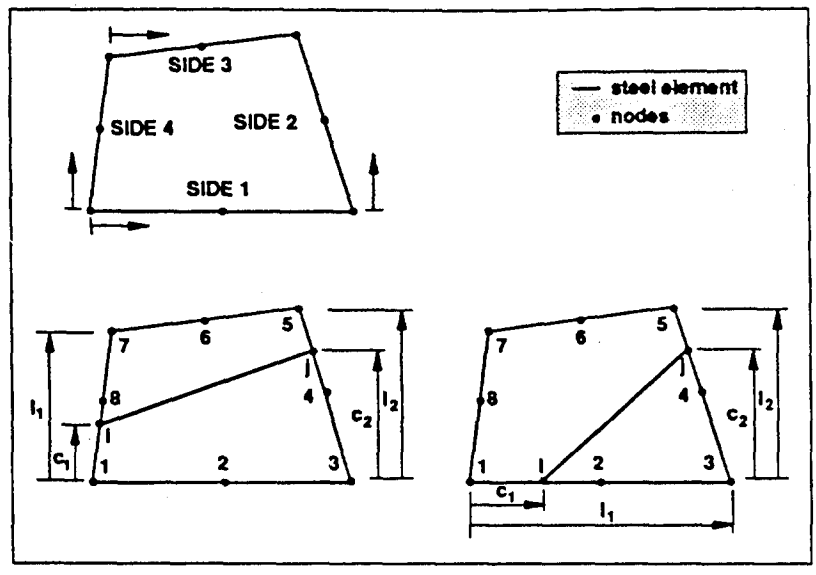

Fig. 6 Steel element embedded in concrete element.

where

$$A_1=\begin{bmatrix} 2p^2-3p+1 & 0 \\ 0 & 2p^2-3p+1 \end{bmatrix} \quad A_2=\begin{bmatrix} -4p^2+4p & 0 \\ 0 & -4p^2+4p \end{bmatrix} \quad A_3=\begin{bmatrix} 2p^2-p & 0 \\ 0 & 2p^2-p \end{bmatrix} \tag{12}$$

$$B_1=\begin{bmatrix} 2q^2-3q+1 & 0 \\ 0 & 2q^2-3q+1 \end{bmatrix} \quad B_2=\begin{bmatrix} -4q^2+4q & 0 \\ 0 & -4q^2+4q \end{bmatrix} \quad B_3=\begin{bmatrix} 2q^2-q & 0 \\ 0 & 2q^2-q \end{bmatrix} \tag{13}$$

$p=c_1/l_1$, $q=c_2/l_2$ and $\mathbf{0}$ is the 2×2 null matrix (Fig. 6). In Eq. (11) the position of sub-matrices $\boldsymbol{A}$ and $\boldsymbol{B}$ within the transformation matrix $[T_2]$ is related to the side of the concrete element which the reinforcing bar element crosses. If the reinforcing bar element crosses the concrete element boundary on sides 1 and 2 in Fig. 6, the transformation matrix $[T_2]$ takes the form:

$$[T_2]=\begin{bmatrix} \boldsymbol{A}_1 & \boldsymbol{A}_2 & \boldsymbol{A}_3 & \mathbf{0} & \mathbf{0} & \mathbf{0} & \mathbf{0} & \mathbf{0} \\ \mathbf{0} & \mathbf{0} & \boldsymbol{B}_1 & \boldsymbol{B}_2 & \boldsymbol{B}_3 & \mathbf{0} & \mathbf{0} & \mathbf{0} \end{bmatrix} \tag{14}$$

noting that the submatrix $\boldsymbol{A}$ and $\boldsymbol{B}$ are the same as before, but c_1 is now defined as shown on the right hand side of Fig. 6.

Moreover an additional step becomes necessary for determining the deformations and forces in the reinforcing steel because the degrees of freedom associated with the reinforcing steel are condenced out of the stiffness matrix in Eq. (5). Once the displacement increments at the nodes of the concrete finite elements are determined for the current load increment, they can be transformed by the matrix $[T_1]$ and $[T_2]$ to yield the concrete displacement increments $\{d_c\}$ at the ends of the steel element in the direction of parallel to the axis of the reinforcing bar. Using the second row of the matrix relation in Eq. (3) which expresses the condition of equilibrium of the reinforcing bar element, the force and deformation increments in steel can now be determined by assembling the steel element matrices and imposing appropriate boundary conditions at the ends of the entire reinforcing bar.

$$[K_{ss}]\cdot\{d_s\}=(\{P_s\}-[K_{cs}]\cdot\{d_c\}) \tag{15}$$

The successive application of this relation along with appropriate conditions for the transition from one element to the next element results in a transfer matrix solution method which offers certain computational advantages over the direct solution method.

3. Solution algorithm for reinforcing steel (Transfer matrix method)

If the reinforcing bar is assumed to be subdivided into n elements, the equilibrium equation of Eq. (15) for the kth element can be represented as Eq. (16):

$$\{\Delta P_s\}^k=[K_{cs}]^k\cdot\{\Delta d_c\}^k+[K_{ss}]^k\cdot\{\Delta d_s\}^k \tag{16}$$

or can be explicitly written as follows:

$$\begin{Bmatrix}\Delta P_2\\ \Delta P_4\end{Bmatrix}^k=\begin{bmatrix}k_s+k_{bi} & -k_s\\ -k_s & k_s+k_{bj}\end{bmatrix}^k\cdot\begin{Bmatrix}\Delta d_2\\ \Delta d_4\end{Bmatrix}^k-\begin{Bmatrix}k_{bi}\cdot\Delta d_1\\ k_{bj}\cdot\Delta d_3\end{Bmatrix}^k \tag{17}$$

where it should be noted that the concrete displacement increments Δd_1 and Δd_3 are known from the global nonlinear finite element analysis of reinforced concrete structures. Solving Eq. (17) for the force and displacement increment at node 4 (Fig. 4) yields:

$$\begin{Bmatrix}\Delta P_4\\ \Delta d_4\end{Bmatrix}^k=[Q]^k\cdot\begin{Bmatrix}\Delta P_2\\ \Delta d_2\end{Bmatrix}^k-[R]^k\cdot\begin{Bmatrix}\Delta d_1\\ \Delta d_3\end{Bmatrix}^k \tag{18}$$

where

$$[Q]^k=\frac{1}{k_s}\begin{bmatrix}-(k_s+k_{bj}) & k_s\cdot(k_{bi}+k_{bj})+k_{bi}\cdot k_{bj}\\ -1 & k_s+k_{bi}\end{bmatrix}^k \tag{19}$$

$$[R]^k=\begin{bmatrix}k_{bi}\cdot\dfrac{k_s+k_{bj}}{k_s} & k_{bj}\\ \dfrac{k_{bi}}{k_s} & 0\end{bmatrix}^k \tag{20}$$

For the transition from the kth to the $(k+1)$th element using the force equilibrium and the compatibility condition, Eq. (21) can be obtained

$$\begin{Bmatrix}\Delta P_2\\ \Delta d_2\end{Bmatrix}^{k+1}=\begin{Bmatrix}-\Delta P_4\\ \Delta d_4\end{Bmatrix}^k=\begin{bmatrix}-1 & 0\\ 0 & 1\end{bmatrix}\cdot\begin{Bmatrix}\Delta P_4\\ \Delta d_4\end{Bmatrix}^k=[S]\cdot\begin{Bmatrix}\Delta P_4\\ \Delta d_4\end{Bmatrix}^k \tag{21}$$

and the substitution of Eq. (18) into Eq. (21) yields the following relation.

$$\begin{Bmatrix}\Delta P_2\\ \Delta d_2\end{Bmatrix}^{k+1}=[\bar{Q}]^k\cdot\begin{Bmatrix}\Delta P_2\\ \Delta d_2\end{Bmatrix}^k-[\bar{R}]^k\cdot\begin{Bmatrix}\Delta d_1\\ \Delta d_3\end{Bmatrix}^k \tag{22}$$

where $[\bar{Q}]^k=[S][Q]^k$ and $[\bar{R}]^k=[S][R]^k$

Eq. (22) relates the force and displacement increments at the beginning of steel element $k+1$ with those of steel element k. By applying Eq. (22) successively to elements $k-1$, $k-2$, ..., 2, 1 and summing up the results, the following transfer matrix relation of Eq. (23) is resulted in:

$$\begin{Bmatrix} \Delta P_2 \\ \Delta d_2 \end{Bmatrix}^{k+1} = [\bar{Q}]^k \cdot \begin{Bmatrix} \Delta P_2 \\ \Delta d_2 \end{Bmatrix}^k - [\bar{R}]^k \cdot \begin{Bmatrix} \Delta d_1 \\ \Delta d_3 \end{Bmatrix}^k$$

$$= [\bar{Q}]^k \cdot [\bar{Q}]^{k-1} \cdot \begin{Bmatrix} \Delta P_2 \\ \Delta d_2 \end{Bmatrix}^{k-1} - [\bar{Q}]^k \cdot [\bar{R}]^{k-1} \cdot \begin{Bmatrix} \Delta d_1 \\ \Delta d_3 \end{Bmatrix}^{k-1} - [\bar{R}]^k \cdot \begin{Bmatrix} \Delta d_1 \\ \Delta d_3 \end{Bmatrix}^k$$

$$= [\bar{Q}]^k \cdot [\bar{Q}]^{k-1} \cdots [\bar{Q}]^1 \cdot \begin{Bmatrix} \Delta P_2 \\ \Delta d_2 \end{Bmatrix}^1 - [\bar{Q}]^k \cdot [\bar{Q}]^{k-1} \cdots [\bar{Q}]^2 \cdot [\bar{R}]^1 \cdot \begin{Bmatrix} \Delta d_1 \\ \Delta d_3 \end{Bmatrix}^1$$

$$- \cdots - [\bar{R}]^k \cdot \begin{Bmatrix} \Delta d_1 \\ \Delta d_3 \end{Bmatrix}^k \tag{23}$$

After replacing $k+1$ with n in Eq. (23) and applying Eq. (18) for element n, the following relation between the forces and displacements at the two ends of the reinforcing bar can be obtained.

$$\begin{Bmatrix} \Delta P_2 \\ \Delta d_2 \end{Bmatrix}^n = [\bar{Q}]^n \cdot [\bar{Q}]^{n-1} \cdots [\bar{Q}]^1 \cdot \begin{Bmatrix} \Delta P_2 \\ \Delta d_2 \end{Bmatrix}^1 - [\bar{Q}]^n \cdot [\bar{Q}]^{n-1} \cdots [\bar{Q}]^2 \cdot [\bar{R}]^1 \cdot \begin{Bmatrix} \Delta d_1 \\ \Delta d_3 \end{Bmatrix}^1$$

$$- \cdots - [\bar{R}]^n \cdot \begin{Bmatrix} \Delta d_1 \\ \Delta d_3 \end{Bmatrix}^n \tag{24}$$

Since one boundary condition is known at each end of the reinforcing steel, after assuming the second boundary condition at the starting end, Eq. (24) yields the force and displacement at the other end of the reinforcing steel. As one condition is known at that end, the initial assumption needs to be corrected until the known boundary condition at the far end is satisfied. It should be noted that the transfer matrix method is applied during the correction phase of the global solution algorithm. Consequently, the transfer matrix relations in Eq. (24) are linear since no updating of the bond and steel stiffness takes place during the correction phase which is based on the initial stiffness method. Thus, Eq. (24) can be solved very rapidly through a series of multiplications and no iteration with the cyclic bond-slip model is required.

The satisfaction of equilibrium of the reinforcing steel by the transfer matrix method of Eq. (24) yields the steel displacement increments. Since the concrete displacements at the ends of the bar are also known for the current load increment, the relative displacements can be readily determined. The state determination of the steel and bond elements can now be undertaken yielding the new steel and bond forces and the updated stiffness matrices. The latter are only needed at the beginning of a new load step, when the stiffness matrix of the structure is updated. The substitution of the new steel and bond forces in Eq. (6) yields the equivalent nodal forces at the global degrees of freedom and the calculated forces are subtracted from the applied load increments to yield the unbalanced forces. The process continues until the convergence criterion is satisfied.

3.1. Convergence criterion

The criterion for measuring the convergence of the iterative solution is based on the accuracy of satisfying the global equilibrium equations or on the accuracy of determining the total displacements. The accuracy of satisfying the global equilibrium equations is controlled by the magnitude of the unbalanced nodal forces. The accuracy of the node displacements depends on the magnitude of the additional displacement increment after each iteration. The latter convergence criterion

is used in this paper. This can be expressed as:

$$E_d = \frac{\left[\sum_j (\Delta d_j^i)^2\right]^{1/2}}{\left[\sum_j (d_j^i)^2\right]^{1/2}} \leq TOLER \tag{25}$$

where the summation extends over all degrees of freedom j, d_j is the displacement of degree of freedom j, Δd_j^i is the corresponding increment after iteration i, and *TOLER* is the specified tolerance.

In the nonlinear analysis of RC structures the load step size must be small enough so that unrealistic "numerical cracking or unstability" does not take place. These numerical unstability can artificially alter the load transfer path within the structure and result in incorrect modes of failure. Crisfield (1982) has shown that such numerical disturbance of the load transfer path after initiation of cracking can give rise to alternative equilibrium states and, hence, lead to false ultimate strength predictions. In order to avoid such problems after crack initiation which means the occurrance of bond-slip, the load is increased in steps of 2.5~5.0% of the ultimate load of the member. The failure load is assumed to occur at a load level for which a large number of iterations are required for convergence. This means that very large strain increments takes place during this step and that equilibrium cannot be satisfied under the applied loads. Obviously, the maximum number of iterations depends on the problem and the specified tolerance, but a maximum of 30 iterations seems adequate for a tolerance of 1%. This is the limit in the number of iterations selected in this study.

4. Numerical examples

In order to test the proposed reinforcing steel model with bond-slip, the response of anchored reinforcing bars under monotonic pull-out and cyclic push-pull loads is studied. Viwathanatepa, Popov and Bertero (1979) tested several anchored reinforcing bars simulating anchorage and loading conditions in interior beam-column joints of moment resisting frames which are subjected to a combinations of gravity and high laterial loads. #6, #8 and #10 reinforcing bars were anchored in well confined concrete blocks and were subjected to monotonic pull-out at one end, monotonic pull-out at one end with simultaneous push-in at the other (called push-pull) and cyclic push-pull.

Two specimens are selected for comparison with the proposed reinforcing steel model with bond-slip. The first specimen is an anchored #8 bar in a well confined block of 25in. (63.5cm) width, which corresponds to an anchorage length of 25 bar diameters. This specimen was subjected to a monotonic pull-out under displacement control at one end only. The second specimen also involves a #8 reinforcing bar with identical dimensions which was subjected to a cyclic push-pull loading with gradually increasing end slip value. Both specimens have been the subject of earlier analytical correlation studies by Viwathanatepa, *et al.* (1979), Ciampi, *et al.* (1982), Yankelevky (1985) and Filippou (1986). The material properties of concrete and reinforcing steel are as fellows: the concrete cylinder strength is 4,700psi (330.5kg/cm^2) for the specimen under monotonic pull-out and 4,740psi (333.3kg/cm^2) for the specimen under cyclic push-pull. The yield strength of the reinforcing steel is 68ksi (4780kg/cm^2), the yield strain is 0.23%, and the modulus of elasticity

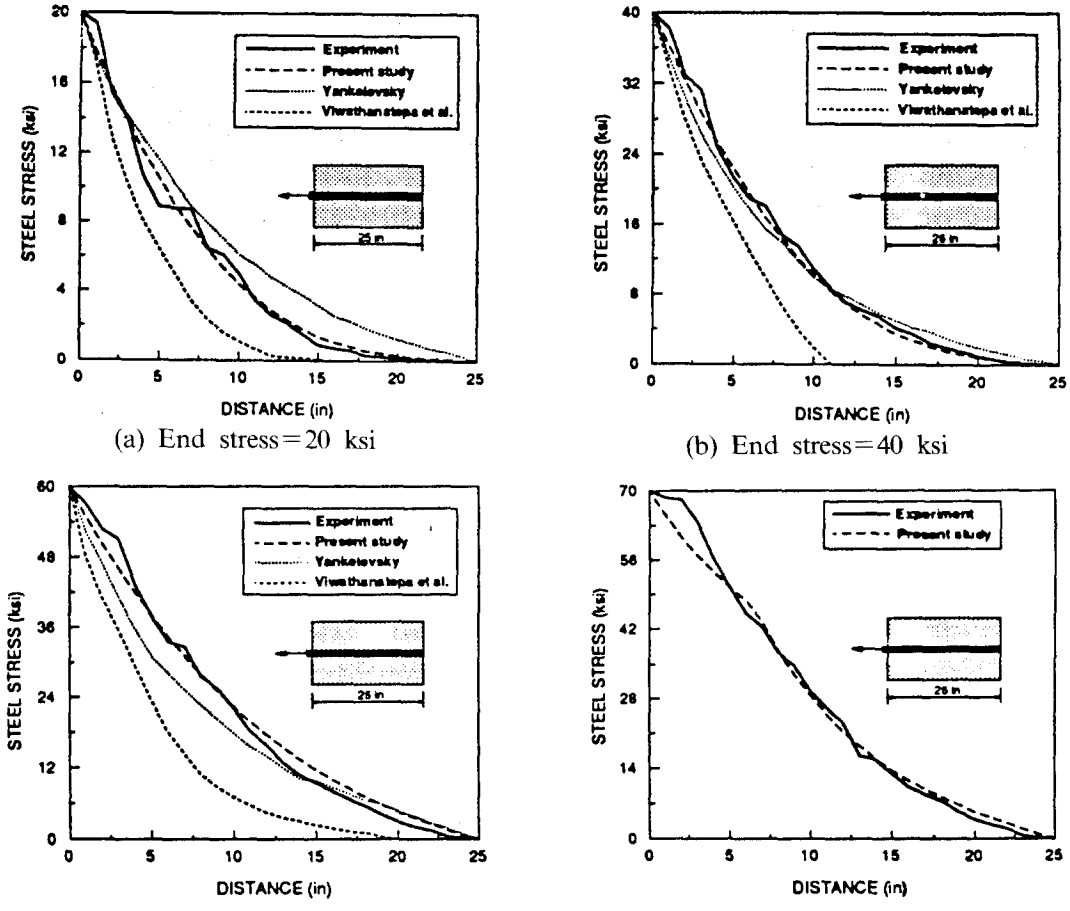

(a) End stress=20 ksi (b) End stress=40 ksi

(c) End stress=60 ksi (d) End stress=70 ksi

Fig. 7 Stress distribution along anchored reinforcing bar.

after yielding is assumed as 411ksi (28,900kg/cm^2). Also the parameters used in the bond model are equal to those used by Filippou, *et al.* (1983) and Filippou (1986) in earlier investigations, namely: u_1=0.02756 in (0.07cm), u_2=0.07874in (0.2cm), u_3=0.2756 in (0.7cm) and τ_1=2350psi (165.2kg/cm^2) (Fig. 3). In the study by Ciampi, *et al.* (1982) the bond-slip relation was modified in the outer unconfined portions along the entire anchorage length. For the sake of simplicity in the present study, the same bond stress-slip relation is used along the entire anchorage length. Under cyclic push-pull loading conditions, this assumption leads to underestimation of the bond resistance at the push-in end of the reinforcing bar. Twenty-five (25) steel elements of 1 inch length were used in modeling the anchored reinforcing bar.

Figs. 7a-7d show the distribution of steel stresses along the anchorage length of the reinforcing bar at different loading stages. The experimental results are compared with the analytical results of Viwathanatepa, *et al.* (1979), Yankelevsky (1985) and those of the present study. The result of the present study shows the best agreement, particularly, with increasing load. It should be noted that the model of Yankelevsky (1985) does not allow for yielding of the reinforcing steel. The results by Viwathanatepa, *et al.* (1979) are from a linear finite element analysis since no stress distributions are presented for the nonlinear model proposed in that study.

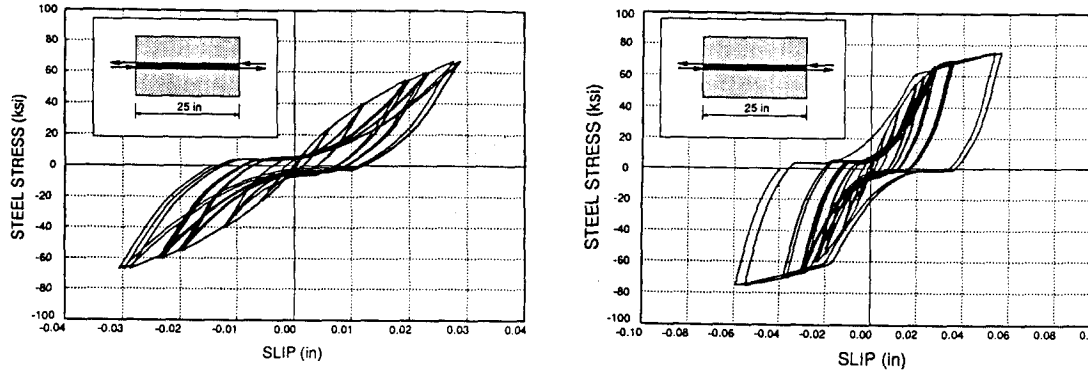

(a) Load cycles before yielding of reinforcing steel (b) Load cycles after yielding of reinforcing steel

Fig. 8 Stress-slip response of anchored reinforcing bar under cyclic push-pull (Analytical results).

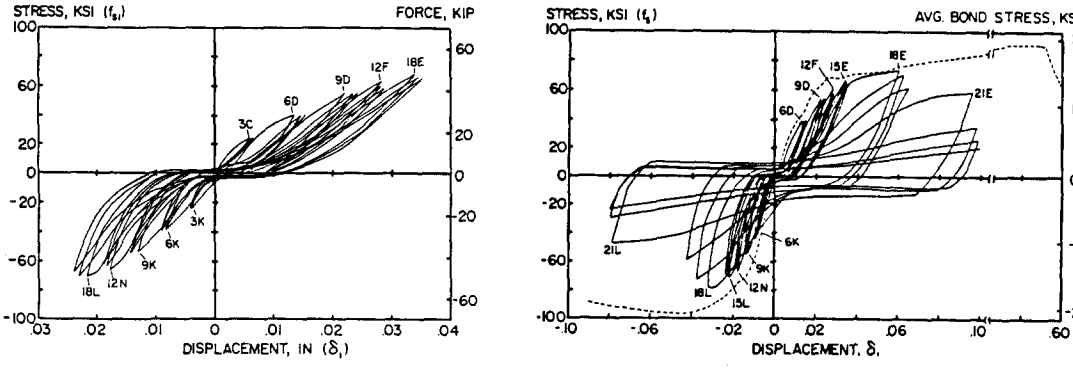

(a) Load cycles before yielding of reinforcing steel (b) Load cycles after yielding of reinforcing steel

Fig. 9 Stress-slip response of anchored reinforcing bar under cyclic push-pull (Experimental results).

Figs. 8a and 8b show the end stress-slip relation of the reinforcing bar under cyclic push-pull loading. Fig. 8a shows the cycles before yielding of the reinforcement and Fig. 8b shows the entire response, and the corresponding experimental data are shown in Figs. 9a and 9b. The steel stress distributions along the anchorage length of the reinforcing bar are shown in Figs. 10a-10f. The experimental results are compared with the analytical results of Viwathanatepa, *et al.* (1979), Yankelevsky (1985) and those of the present study. The results of the proposed model show an excellent agreement with experimental results in the early cycles in Figs. 10a-10f. However, the comparison of the overall response in Figs. 8 and 9 shows small discrepancies between the present model and the experimental data as the loading increases. Two factors are attributable to this: (1) the present model is tested under load controlled conditions while the experimental specimen was subjected to displacement controlled testing, and (2) the assumption that the bond stress-slip relation is the same along the anchorage length of the bar is not adequate for the large deformation stage where a significant bond damage can occur. It is concluded that the proposed reinforcing steel model with bond-slip can describe quite well the response of anchored reinforcing bars under monotonic and cyclic loading conditions.

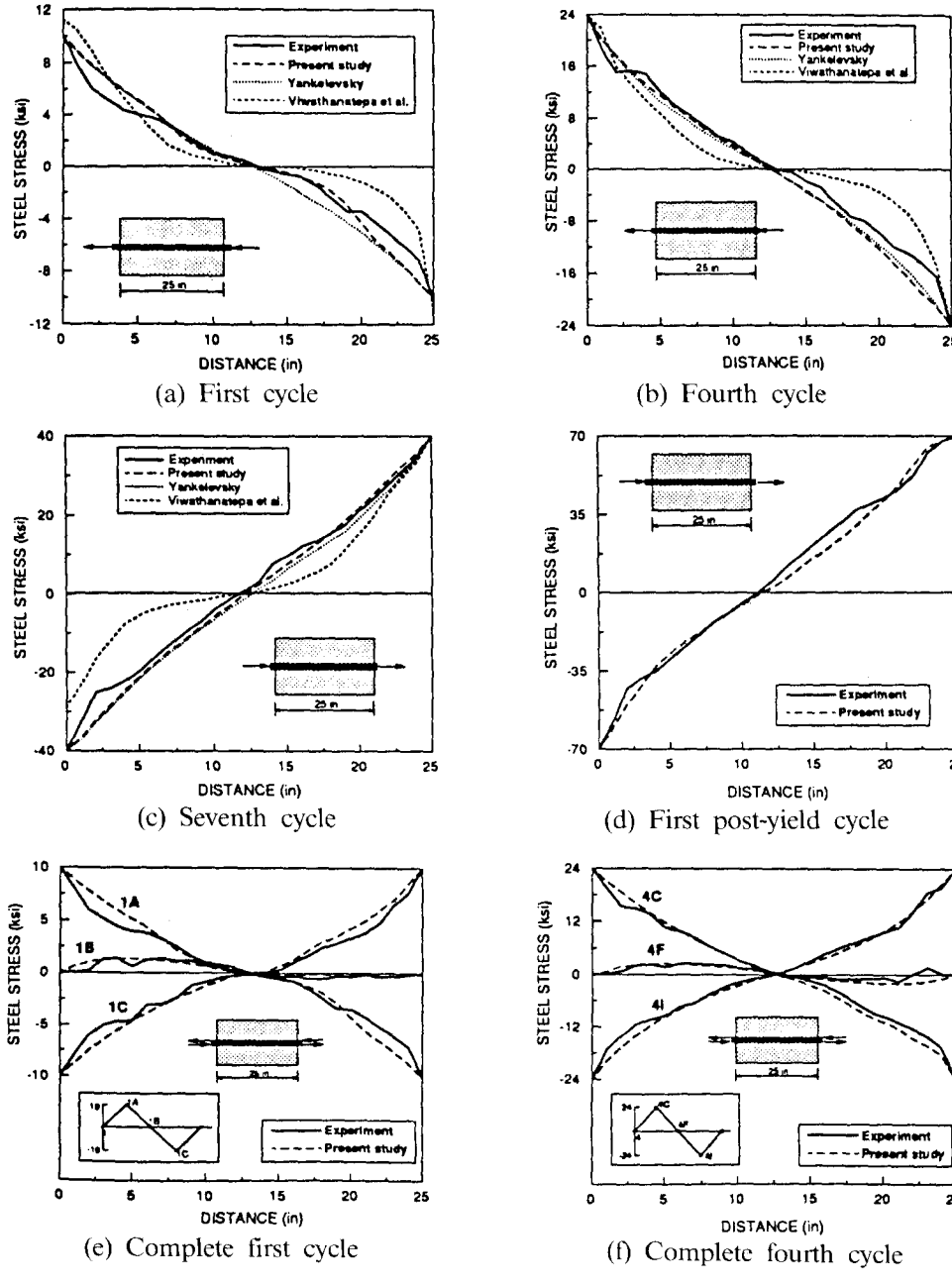

Fig. 10 Stress distribution along anchored reinforcing bar under cyclic push-pull loading.

5. Conclusions

An improved numerical approach to consider the bond-slip effect without taking double nodes is proposed. Unlike the classical bond-link and bond-zone element which have the restrictions in the numerical modeling such as a reinforcing bar arrangement along the edge of a concrete element and a double node to represent the relative slip between reinforcing steel and concrete,

the proposed model which does not take the double nodes can yield significant savings in the number of nodes needed to account for the effect of bond-slip, particulary, in three dimensional finite element models. A new nonlinear solution scheme based on the equilibrium at each node of steel and the compatibility condition between steel and concrete is developed in connection with this model. The efficiency and reliability of the proposed model are demonstrated through the correlation studies between analytical and experimental results under both monotonically increasing and repeated large deformation stages.

References

ASCE Task Committee on Finite Element Analysis of Reinforced Concrete Structures (1982), *State-of-the-Art Report on Finite Element Analysis of Reinforced Concrete, ASCE* Special Publications.

Ciampi, V., Eligehausen, R., Popov, E.P. and Bertero, V.V. (1982), "Analytical model for concrete anchorages of reinforcing bars under generalized excitations", *Report No. UCB/EERC-82/23*, Earthquake Engineering Research Center, University of California, Berkeley.

Choi, C.K. and Kwak, H.G. (1990), "The effect of finite element mesh sizes in nonlinear finite element analysis of R/C structures", *Computers and Structures*, **36**(4), 175-186.

Crisfield, M.A. (1982), "Accelerated solution techniques and concrete cracking", *Computer Methods in Applied Mechanics and Engineering*, **33**, 585-607.

de Groot, A.K., Kusters, G.M.A. and Monnier, T. (1981), "Numerical modeling of bond-slip behavior", *Heron, Concrete Mechanics*, **26**(1B).

Eligehausen, R., Popov, E.P. and Bertero, V.V. (1983), "Local bond stress-slip relationships of deformed bars under generalized excitations", *Report No. UCB/EERC 83-23*, Earthquake Engineering Research Center, University of California, Berkeley.

Filippou, F.C. (1986), "A simple model for reinforcing bar anchorages under cyclic excitations", *Journal of Structural Engineering, ASCE*, **112**(7), 1639-1659.

Filippou, F.C., Popov, E.P. and Bertero, V.V. (1983), "Effects of bond deterioration on hysteretic behavior of reinforced concrete joints", *Report No. UCB/EERC-83/19*, Earthquake Engineering Research Center, University of California, Berkeley.

Hayashi, S. and Kokusho, S. (1985), "Bond behavior in the neighborhood of the crack", *Proceedings of the U.S.-Japan Joint Seminar on Finite Element Analysis of Reinforced Concrete*, 364-373, Tokyo, Japan.

Keuser, M. and Mehlhorn, G. (1987), "Finite element models for bond problems", *Journal of Structural Engineering, ASCE*, **113**(10), 2160-2173.

Kwak, H.G. and Filippou, F.C. (1990), "Finite element analysis of reinforced concrete structures under monotonic loads", *Report No. UCB/SEMM-90/14*, University of California, Berkeley.

Menegotto, M. and Pinto, P. (1973), "Method of analysis for cyclically loaded reinforced concrete plane frames including changes in geometry and nonelastic behavior of elements under combined normal force and bending", *IABSE Symposium on Resistance and Ultimate Deformability of Structures Acted on by Well-Defined Repeated Loads*, Final Report, Lisbon.

Ngo, D. and Scordelis, A.C. (1967), "Finite element analysis of reinforced concrete beams", *Journal of ACI*, **64**(3), 152-163.

Viwathanatepa, S., Popov, E.P. and Bertero, V.V. (1979), "Seismic behavior of reinforced concrete interior beam-column subassemblages", *Report No. UCB/EERC-79/14*, Earthquake Engineering Research Center, University of California, Berkeley.

Yankelevsky, D.Z. (1985), "New finite element for bond-slip analysis", *Journal of Structural Engineering, ASCE*, **111**(7), 1533-1542.

Zulfiqar, N. and Filippou, F.C. (1990), "Models of critical regions in reinforced concrete frames under seismic excitations", *Report No. UCB/EERC-90/06*, Earthquake Engineering Research Center, University of California, Berkeley.